

European Option Pricing with a Fast Fourier Transform Algorithm for Big Data Analysis

Abstract — Several empirical studies show that, under multiple risks like stochastic volatility and jump risks, markets exhibit many new properties, such as volatility smile and cluster fueled by the explosion of transaction data. The traditional Black-Scholes model fails to fit these newly-developed characteristics. This paper attempts to capture these newer features, using the valuation of European options as a vehicle. Statistical analysis performed on the data collected from the currency option market clearly shows the existence of mean reversion, jumps, volatility smile, and leptokurtosis and fat tail. We characterize the dynamics of the underlying asset in this kind of environment by establishing a coupled stochastic differential equation model with triple characteristics of mean reversion, non-affine stochastic volatility and mixed-exponential jumps. However, the traditional no-arbitrage option pricing theory no longer applies for analytical solution of this model. Moreover, the commonly used Monte Carlo simulation to numerically calculate the option prices takes a long time, especially for a huge amount of data. We propose a characteristic function method to derive the closed-form pricing formula. We also present a Fast Fourier Transform (FFT) algorithm-based numerical solution method. Finally, extensive numerical experiments are conducted to validate both the modeling methodology and the numerical algorithm. Results demonstrate that the model behaves well in capturing the properties observed in the market, and the FFT numerical algorithm is both accurate and efficient in addressing large amount of data.

Index Terms — Multiple risks; European option pricing; stochastic modeling; Fast Fourier Transform algorithm; big data analysis.

I. INTRODUCTION

OPTION is being increasingly used as a very important contract for hedging and risk aversion in both financial and operational markets. The Shanghai Stock Exchange issued the first option in the Chinese financial market, called the 50ETF option, on February 9, 2015. In the global industrial procurement, the option contract is commonly used to avoid various kinds of risks, such as price, demand, and foreign exchange rate risks. Therefore, valuing the options more accurately and quickly is of great importance, especially in the big data era.

The best-known among all the option pricing theories is the Black-Scholes (BS) formula derived by Black and Scholes (1973) [1]. This formula greatly promoted both the application of options in the market and the rapid development of option theories. Until around 1986, the BS pricing model was proven to be able to depict the market very well. However, the applicability of this model was later widely questioned as a series of mishaps occurred in the financial markets. Prominent among them were the Asian financial crisis during the 1990s and the subprime crisis and the subsequent failure of the Lehman Brothers in the early 21st century. In fact, the traditional BS model does not work when the market risks, such as stochastic volatility and jump risks, increase. Another new development is the advent of the big data era where bulk data handling techniques enable

the collection and processing of big and high-frequency data. Many empirical studies show that the mass and high-frequency data demonstrate new properties of the option market, such as leptokurtosis and fat tail, volatility smile, asymmetric distribution, and volatility cluster. To explain these phenomena, many researchers have improved the classical BS model with various methods. We include a review of these improved models in Section II.

In this paper, we propose an adaptable modeling methodology that could better capture the new properties of the underlying asset when multiple risks exist. We also present an effective and efficient option pricing method to provide a useful tool for practice. We consider the European option pricing issue as a vehicle of analysis. Traditionally, researchers have developed their solution methods under a number of restrictive assumptions (as detailed later) in order to make the models tractable. We make only three assumptions that are not over-restrictive and do not take away from the usability of the results. Our first assumption is that the short-term interest rate is constant. Secondly, there are no transaction costs or taxes. Finally, the market pays no dividends or other distributions. A more detailed description of these assumptions is given later in Section IV. Based on these assumptions, we establish a coupled dynamic model for the log underlying asset under risk neutral measures. We are able to obtain both analytical and numerical solutions for the European option pricing problem. This paper has the following four main contributions:

- 1) Using a series of empirical performance based on statistical analysis, we demonstrate that, under multiple risks, certain kinds of markets like the currency option market show the characteristics of mean reversion, jumps, volatility smile, and leptokurtosis and fat tail simultaneously. This is shown in Section III.
- 2) Based on the empirical evidences, the classic BS modeling structure and some relevant research literature, we use the methods of stochastic equations and analyses and establish a general European option pricing model under risk neutral measures. We prove through a series of numerical experiments that our triple-characteristic stochastic model is able to well-describe the new market properties mentioned above, namely mean reversion, jumps, volatility smile, and leptokurtosis and fat tail.
- 3) With the methods of characteristic function initially proposed by [2], we derive the approximate analytical solution for the European option by adopting a number of mathematical tools, such as the generalized Feynman-Kac formula, nonlinear perturbation analysis, and solution techniques for the Riccati equation.
- 4) Basing on the analytical solution, we develop a Fast Fourier Transform (FFT) algorithm (first introduced by [3]) to obtain a numerical solution method that does well in addressing large amounts of data. Our numerical experiments demonstrate that the FFT algorithm-based numerical solution method is both effective and efficient compared with performance of traditional Difference Monte Carlo (DMC) simulation.

The remainder of this paper is organized as follows. We review the literature related to our paper in Section II. Section III provides empirical evidences to demonstrate the validity of the model proposed in this paper. In Section IV, we lay out the basic model for the log underlying asset with properties of mean reversion, non-affine stochastic volatility, and mixed-exponential jumps. In Section V, we introduce our European options pricing model, both analytically and numerically. In Section VI, we show parts of the results from our extensive numerical experiments. Section VII concludes this paper and indicates some future research directions.

II. SURVEY OF RELATED LITERATURE

There are three main issues related to our paper, namely background, modeling and calculation. Our research was conducted based on the market risk analysis under the environment of big data, and our models were established on the basis of the existing option pricing methods. Moreover, the proposed numerical algorithm for model calculation was greatly inspired by previous works. Therefore, we carry on a thorough literature review in the three dimensions: risk analysis, modeling methods and numerical algorithms.

A. Risk Analysis

There are a variety of risks that widely exist in different systems. Additionally, as the systems develop, many new kinds of risks emerge. Risk analysis, therefore, is a very important research topic. Several papers have focused on exploring new methods to effectively identify, evaluate and control risks. For example, Choi explored the risk levels of a two-echelon supply chain system with vendor managed inventory scheme, and concluded that the RFID technology could improve the supply chain resulting in both larger expected profit and smaller risk [4]. Large-scale integration of renewable energies causes a higher degree of volatility and uncertainty of power flows in the electrical transmission system, giving a higher risk of cascading line outages. Muller et al. proposed a novel approach for a distributed real-time coordination and effectively controlled the risks in power flow [5]. Especially, option contract is a very common and useful tool among all kinds of risk controlling strategies. For instance, Asian and Nie designed an option contract to cope with the global supply network risks caused by market volatility and supply disruptions [6]. Shi and Min proposed a real option approach to control the cost uncertainty risk by allowing a firm to decide when to replace the leased product and remanufacture it [7].

B. Modeling Methods

The traditional BS model was established under many assumptions. Both the expected return of the underlying asset and its volatility were presumed to be constants. Moreover, it was assumed that the curve of the underlying asset price was continuous. However, these assumptions are widely questioned by series of practical observations and empirical research works. Therefore, many papers have attempted to improve the BS model from different perspectives. Generally, these modeling methods may fall into three categories, namely, mean reversion models, stochastic volatility models and jump models. To capture the mean reversion character observed in markets like commodity, Hahn and Dyer utilized a more general binomial approximation methodology to model simple homoscedastic mean-reverting stochastic processes as recombining lattices for real option valuation [8].

Also, “volatility smile” is a well-known phenomenon. To address this problem, many scholars have explored various modeling methods,

among which stochastic volatility models are most widely recognized. For example, Park and Kim investigated a semi-analytic pricing method for lookback options in a general stochastic volatility framework [9]. Nearly all the stochastic volatility models are affine. However, some papers recently found that the non-affine property of the financial time series existing in reality could not be well described. As a result, a growing number of scholars have started focusing on pricing options with the models of non-affine stochastic volatility. For instance, Yuen and Zheng considered pricing of various types of exotic discrete variance swaps, like the gamma swaps and corridor variance swaps, under the 3/2 non-affine stochastic volatility models [10].

Moreover, in practice, various kinds of jumps exist widely in the markets because of factors like wars, economic crises, and real-time market trading. Option pricing problems where the dynamic process of the underlying asset follows a jump diffusion model have been well researched. A generalized jump-diffusion model was proposed to price European vulnerable options by Fard, and a closed-form price solution was derived by Esscher transform [11]. Furthermore, some papers study option pricing with underlying assets simultaneously exhibiting two kinds of the three properties mentioned above. For example, Chung and Wong investigated analytical pricing of discrete arithmetic Asian options with mean reversion and jumps [12], while Mayer et al. modeled electricity spot prices combining mean reversion and stochastic volatility [13].

C. Numerical Algorithms

Adaptable numerical algorithm for option pricing is another branch of literature closely related to our research. Rapid and accurate pricing of the options, especially in the era of big data, is of great importance in practice. Researchers have been exploring both traditional and modern numerical algorithms for option pricing models. Several studies have focused on modern algorithms. For example, Gradojevic et al. investigated a nonparametric modular neural network (MNN) model to price the S&P-500 European call options [14]. Most studies focus on the traditional algorithms, though. For instance, Tse et al. presented a novel parallel architecture for accelerating quadrature methods used for pricing complex multi-dimensional options [15]. Zhou proposed a new approximate value iteration method, namely near-value iteration, to solve continuous-state optimal stopping problems under partial observation [16]. Especially, as a very efficient algorithm, FFT was widely applied in various areas, such as [17], [18] in signal processing as well as [19] in defense and security systems. Carr and Madan successfully introduced the FFT into option pricing [3].

Relying on risk analysis methods presented in Section II-A, we analyze various emerging risks in the big data era, and capture some simultaneously exhibited properties in certain market, which inspire and lay a solid basis for the subsequent modeling and calculation research works. The models reviewed in Section II-B improved the classical BS model through capturing one or two of the several data characteristics. Based on the studies above, we combine the triple characteristics of mean reversion, non-affine stochastic volatility, and mixed-exponential jumps to establish a general stochastic model. To the best of our knowledge, this type of general stochastic model has not been adequately explored before. Our model is able to depict the phenomena of mean reversion, jumps, volatility smile, leptokurtosis and fat tail, which are simultaneously observed in some markets like the foreign currency option market. This will be detailed in Section III. Moreover, using the FFT algorithm-based method proposed in Section II-D, we obtain an effective and efficient numerical solution for the proposed model.



Fig. 1. Historical data series for foreign exchange rates of EURGBP and EURUSD from January 1, 2001 to May 18, 2015

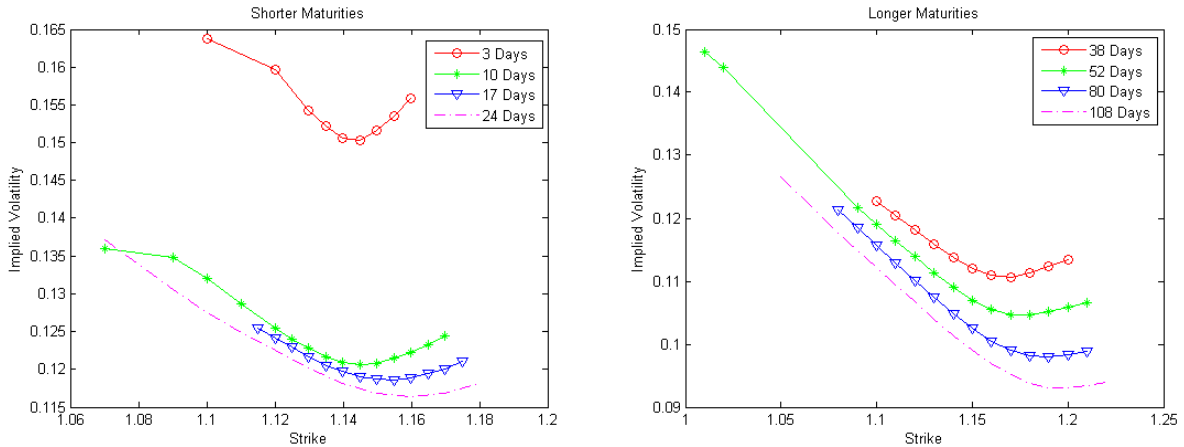


Fig. 2. Market implied volatility smiles for different maturities, one figure for shorter maturities and the other for longer maturities.

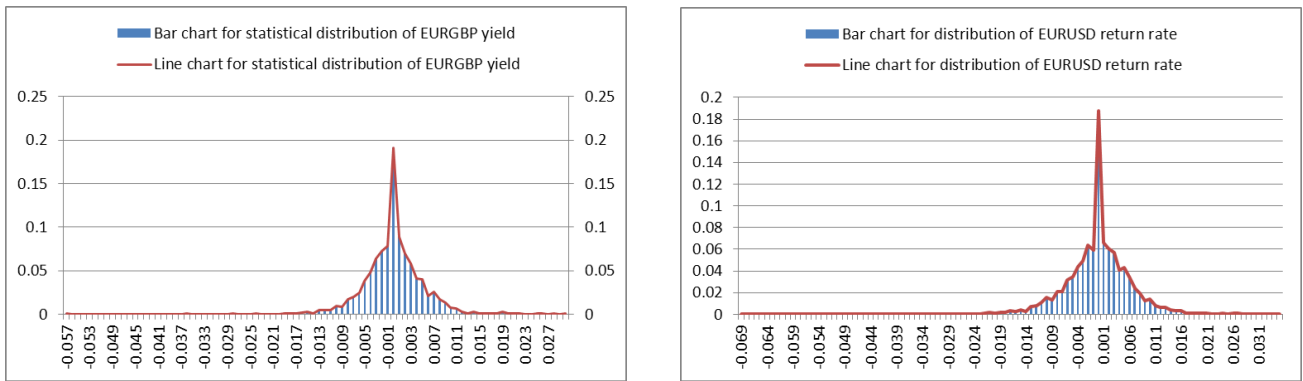


Fig. 3. Statistical distributions for the daily yields of EURGBP and EURUSD foreign exchange rates.

III. EMPIRICAL EVIDENCE

In this section, we conduct some statistical analysis to show the simultaneous occurrence of mean reversion, jumps, volatility smile, and leptokurtosis and fat tail in data from real life. To do that, we use data from the currency option market collected from the Saxo Trader platform.

A. Mean Reversion and Jumps Phenomenon

To present the phenomenon of mean reversion and jumps, we collected the daily mid-quotes of EURGBP and EURUSD foreign exchange rates for the period between January 1, 2001 and May 18, 2015 as shown in Fig. 1, which visually shows significant mean-reversion characteristics of both EURGBP and the EURUSD.

Using the EURUSD as an example, the data shows that the Euro maintained a distinct depreciation trend relative to the Dollar from January 1, 2001 through June 2001. Subsequently, the Euro exchange rate increased rapidly until November 2001. In the following 12 years, the Euro exchange rate underwent a number of appreciations and depreciations with respect to the dollar. EURGBP shows similar trends. Additionally, jumps are seen to be obviously occurring frequently in the historical data. We see the exchange rate jumping up, and at other times jumping down. This shows that it is very important to include mean reversion and jumps into any option price modeling..

B. Volatility Smiles Phenomenon

In order to illustrate the volatility smile phenomenon, we collected

data of the observed implied volatilities of the foreign exchange

TABLE I
LIST OF SYMBOLS

| Symbol | Description |
|---|--|
| $E^Q[\cdot]$ | Expectation function under risk neutral measure Q . |
| (Ω, \mathcal{F}, P) | Real probability space. |
| (Ω, \mathcal{F}, Q) | Probability space under risk neutral measure Q . |
| T | Delivery time of a European option. |
| K | Exercise price of a European option. |
| $C(\cdot)$ | European option price function. |
| C_0 / C_T | European option price at time $0/T$. |
| t/u | Time, $t/u \in [0, T]$. |
| $S_t / S_u / S_0 / S_T$ | Underlying asset price at time $t/u/0/T$. |
| S_{t-} / S_{u-} | Value of S_t / S_u before a jump happens at time t/u . |
| S_t^c / S_u^c | Continuous part of S_t / S_u . |
| v_t / v_0 | Volatility of the underlying asset price at time $t/0$. |
| κ / κ^* | Mean reverting intensity of the underlying asset under different probability measures. |
| θ / θ^* | Equilibrium mean level of the asset against time under different probability measures. |
| a / a^* | Equilibrium mean level of the volatility process against time under different probability measures. |
| b / b^* | Mean reversion speed of the volatility process under different probability measures. |
| σ | Constant volatility coefficient of the volatility process. |
| ρ | Correlation coefficient for the two Brownian motions. |
| W_t^1 / W_t^2 | Two correlated Brownian motions with correlation coefficient ρ in real probability space. |
| W_t^{1*} / W_t^{2*} | Two Brownian motions corresponding to W_t^1 / W_t^2 under risk neutral measure. |
| $\{V_i\}$ | A set of nonnegative stochastic variables, representing the percentage of jump amplitude. |
| J | A stochastic variable representing the jump amplitude, which follows a mixed-exponential distribution. |
| λ | Jump intensity, $\lambda > 0$. |
| $p_u / p_i / \eta_i / q_u / q_j / \theta_j$ | The relevant parameters defined in a mixed-exponential distribution. |
| N_t | Poisson process with jump intensity $\lambda > 0$ defined in real probability space. |
| N_t^* | Poisson process corresponding to N_t under risk neutral measure. |
| $X_t / X_u / X_u$ | Log underlying asset price at time $t/u/T$. |
| X_{t-} / X_{u-} | Value of X_t / X_u just before a jump happens at time t/u . |
| X_t^c / X_u^c | Continuous part of X_t / X_u . |
| $\phi_{X_t E}(\cdot) / \phi_T$ | Characteristic function of log underlying asset price. |
| $F_{k,u}^{-1}(\cdot)$ | Inverse Fourier transformation function. |
| α | The modifying factor and $\alpha > 0$. |
| r | Risk free interest rate. |
| k | Log exercise price. |
| $M(\cdot, \cdot) / W(\cdot, \cdot)$ | Two Whittaker functions. |
| N | Sectional number of a given interval for exercise price |
| M | Sample size for Difference Monte Carlo simulation. |
| $l/h/j$ | Counting variable. |
| Δ/l | Step length for different intervals. |
| $C(t, T) / D(t, T) / B(t, T) / \varphi(u) / w(\cdot) / x(\cdot) / f(\cdot)$ | Intermediate functions during derivation process. |
| $p/q/s/p^*/q^*$ | Intermediate variables during derivation process. |
| y/u | Intermediate variables during derivation process. |

options written on EUR/USD from the trading platform. An example of observed implied volatilities for eight different time-to-maturities on May 18, 2015 is presented in Fig. 2. We observe an obvious volatility smile phenomenon for the currency options, both in short maturities of 3, 10, 17 and 24 days and in long maturities of 38, 52, 80 and 108 days. These empirical evidences strongly suggest that option pricing models should be sufficiently flexible to capture not only the mean reversion and jumps but also the volatility smile.

C. Leptokurtosis and Fat Tail Phenomenon

To figure out whether the leptokurtosis and fat tail phenomenon exists in the currency option market, we conducted statistical analysis on the daily mid-quotes of EURGBP and EURUSD foreign exchange rates from January 1, 2006 through to May 18, 2015. We calculated the daily yields of EURGBP and EURUSD respectively, and plotted their distributions in Fig. 3. It shows that both the distributions of EURGBP and EURUSD foreign exchange rates are leptokurtosis and have fat tail. More specifically, we calculated that the kurtosis for the two distributions are 9.37 and 7.70 respectively, which were much larger than 3.00, the kurtosis for normal distributions. Thus, one can infer that the leptokurtosis and fat tail phenomenon does exist in the currency option market. This analysis motivates us to include the characteristic of leptokurtosis and fat tail when modeling the dynamics of the underlying asset.

IV. BASIC MODEL FOR UNDERLYING ASSET

In this section, we establish a basic stochastic model for the price of an underlying asset. For readability, we have presented all the mathematical symbols and their descriptions in this paper in Table I. As mentioned earlier in Section I, we use the following three assumptions in our modeling.

Assumption 1. The short-term risk-free interest rate is known and constant through time.

Assumption 2. The market is frictionless, i.e., there are no transaction costs or taxes in the market.

Assumption 3. The market does not pay dividends or other distributions.

Compared to the classical five assumptions normally used for the market of underlying asset (refer to [1]), the assumptions proposed here are much weaker. Owing to the pricing methods adopted, we do not have to assume that it is possible to borrow any fraction of the price of a security to buy it or to hold it at the short-term interest rate or there are no penalties to short selling as done in [1]. These three assumptions are used to simplify the model setting and make it more tractable so as to generate meaningful managerial guidelines. Our main results would still hold if these assumptions are relaxed. In case these assumptions are relaxed, the pricing results would surely be more accurate since the basic model would be more consistent with the real life situation. However, in this paper, we mainly focus on providing a modeling methodology which would better characterize the concurrent properties present in some markets mentioned in the previous sections. The three factors referred in the assumptions are not the key points related to the market properties being considered, so these assumptions do not take away anything from our analysis of the real life situation.

We now build the basic log asset price model under the classical BS structure. As detailed in our literature review, many scholars have explored different ways to improve the classic BS model in order to reflect the new features of the market. Several of these main

TABLE II
DYNAMIC MODELS FOR OPTION PRICING

| Pricing models | Dynamics |
|----------------------------------|--|
| Black Scholes model (BS) | $dS_t = \mu S_t dt + \sigma S_t dW_t$ |
| Mean Reversion model (MS) | $dS_t = \kappa(\theta - \ln S_t)S_t dt + \sigma S_t dW_t$ |
| Stochastic Volatility model (SV) | $\begin{cases} dS_t = \mu S_t dt + \sqrt{v_t} S_t dW_{1t} \\ dv_t = \kappa(\theta - v_t)dt + \sigma v_t dW_{2t} \end{cases}$ |
| Normal Jump model (NJ) | $\begin{cases} dS_t = \mu S_t dt + \sigma S_t dW_t + JS_t dN_t \\ J \sim \text{Normal}(a, b) \end{cases}$ |

The models are illustrated under objective measures.

categories are shown in Table II. However, through statistical analysis on empirical data, we demonstrated that the phenomena of mean reversion, jumps, volatility smile, and leptokurtosis and fat tail do simultaneously occur in some markets. As mentioned, our aim in this paper is to establish a model which could characterize the properties of these markets. To depict the mean reversion feature, we take the mean reversion item into our model based on the MS model. Also, SV models offer a good approach to address the volatility smile/skew, and according to literature, non-affine stochastic volatility model has better description effect than the traditional affine one. Therefore, we adopt a non-affine stochastic process to model the dynamics of the volatility. Moreover, compared to the NJ models, the mixed-exponential distributions can approximate any distribution as closely as possible and thus could simulate various kinds of big and small jumps existing in the market. Hence, we model the jump phenomenon with mixed-exponential jumps.

On the basis of the above analysis, we build a coupled stochastic equation model with triple characteristics of mean reversion, non-affine stochastic volatility, and mixed-exponential jumps (hereafter referred to as the ‘‘triple characteristics model’’). The following steps derive our basic model.

A. Basic Model without Jumps

Assume that the underlying asset price S_t and the corresponding volatility v_t follow the dynamic model below:

$$dS_t = \kappa(\theta - \ln S_t)S_t dt + \sqrt{v_t} S_t dW_t^1 \quad (1)$$

$$dv_t = b(a - v_t)dt + \sigma v_t^{\eta/2} dW_t^2 \quad (2)$$

$$dW_t^1 dW_t^2 = \rho dt \quad (3)$$

where θ is a constant representing the equilibrium mean level of the asset against time, κ is the mean reverting intensity of the assets, a is a constant standing for the equilibrium mean level of the volatility process against time, and b is the mean reversion speed of the volatility process. σ is the constant volatility coefficient of the volatility process. For the stochastic differential equation (2) to be well-behaved, we select $\eta \in [0, 2]$, representing the non-affine volatility coefficient of the volatility process. W_t^1 and W_t^2 are two correlated Brownian motions with correlation coefficient ρ defined in the real probability space (Ω, \mathcal{F}, P) .

B. Triple Characteristics Model

We assume that N_t is a Poisson process defined in the real probability space (Ω, \mathcal{F}, P) with jump intensity coefficient $\lambda > 0$ and is independent from W_t^1 and W_t^2 . $\{V_i\}$ is a set of nonnegative

stochastic variables which are independent from each other and have identical distributions, representing the percentage of jump amplitude.

Let $J = \log(V)$, then J follows a mixed-exponential distribution:

$$J \square MEJ(p_u, p_i, \eta_i, q_d, q_j, \theta_j), \quad i = 1, 2, \dots, n_1; \quad j = 1, 2, \dots, n_2.$$

with density function as follows:

$$g_j(y) = p_u \sum_{i=1}^{n_1} p_i \eta_i e^{-\eta_i y} 1_{\{y \geq 0\}} + q_d \sum_{j=1}^{n_2} q_j \theta_j e^{\theta_j y} 1_{\{y < 0\}}$$

where $p_u \geq 0, q_d \geq 0, p_u + q_d = 1$, stands for the probabilities that the underlying asset price jumps upward and downward, and

$$p_i \in (-\infty, +\infty), \quad \text{for } \forall i = 1, \dots, n_1, \quad \sum_{i=1}^{n_1} p_i = 1;$$

$$q_j \in (-\infty, +\infty), \quad \text{for } \forall j = 1, \dots, n_2, \quad \sum_{j=1}^{n_2} q_j = 1;$$

$$\eta_i > 1, \quad \text{for } \forall i = 1, \dots, n_1; \quad \theta_j > 0, \quad \text{for } \forall j = 1, \dots, n_2.$$

As p_i and q_j could be negative, these parameters should satisfy certain conditions to guarantee that the density function $g_j(y)$ is both nonnegative and a probability density function. One necessary requirement is: $p_i > 0, q_i > 0, \sum_{i=1}^{n_1} p_i \eta_i \geq 0$, and $\sum_{j=1}^{n_2} q_j \theta_j \geq 0$. One simple

sufficient condition is: $\sum_{i=1}^k p_i \eta_i \geq 0, \quad \text{for } \forall k = 1, \dots, n_1,$ and

$\sum_{j=1}^l q_j \theta_j \geq 0, \quad \text{for } \forall l = 1, \dots, n_2.$ To ensure that S_t has a finite

expectation, the conditions $\eta_i > 1$ for $\forall i = 1, \dots, n_1$, and $\theta_j > 0$, for $\forall j = 1, \dots, n_2$, are necessary. Then the triple characteristics model with jumps is derived as follows:

$$dS_t = \kappa(\theta - \ln S_t)S_t dt + \sqrt{v_t} S_t dW_t^1 + (e^J - 1)S_t dN_t \quad (4)$$

$$dv_t = b(a - v_t)dt + \sigma v_t^{\eta/2} dW_t^2 \quad (5)$$

$$dW_t^1 dW_t^2 = \rho dt \quad (6)$$

Other parameters are as explained in the model labeled (1)–(3).

C. Model Transformation under Risk Neutral Measure

According to the Girsanov theorem, a risk neutral measure Q exists. In the space under risk neutral measure (Ω, \mathcal{F}, Q) , assume that the risk premium is a linear function of the variance [2], that is, $\delta(S_t, v_t, t) = \delta v_t$. Let:

$$\begin{aligned} m &= E^Q[V - 1] \\ &= E^Q[e^J - 1] = p_u \sum_{i=1}^{n_1} \frac{p_i \eta_i}{\eta_i - 1} + q_d \sum_{j=1}^{n_2} \frac{q_j \theta_j}{\theta_j + 1} - 1. \end{aligned}$$

Then the models labeled (4)–(6) are transformed as follows through measure transformation:

$$dS_t = \kappa^* (\theta^* - \ln S_t - \frac{\lambda m}{\kappa^*}) S_t dt + \sqrt{v_t} S_t dW_t^{1*} + (e^J - 1) S_t dN_t^* \quad (7)$$

$$dv_t = b^* (a^* - v_t) dt + \sigma v_t^{\eta/2} dW_t^{2*} \quad (8)$$

$$dW_t^{1*} dW_t^{2*} = \rho dt \quad (9)$$

where $\kappa^* = \kappa + \delta, \theta^* = \frac{\kappa \theta}{\kappa + \delta}, b^* = b + \delta, a^* = a + \frac{ab}{a + \delta}, W_t^{1*}$ and W_t^{2*} are the standard Brownian motions under risk neutral measure Q with correlation coefficients $\text{corr}(dW_t^{1*}, dW_t^{2*}) = \rho$.

D. Derivation of the Basic Log Asset Price Model

To derive the pricing formula for European options with the

underlying asset following dynamics (7)–(9) using the characteristic function method, the characteristic function for the log asset price needs to be determined first. Therefore, we define a new stochastic process $\{X_t, t \geq 0\}$ as follows:

$$X_t = \ln S_t \quad (10)$$

Using the Itô-Doeblin formula, we obtain the following:

$$X_t = X_0 + \int_0^t \frac{1}{S_u} dS_u^c - \frac{1}{2} \int_0^t \frac{1}{S_u^2} dS_u^c dS_u^c + \sum_{0 \leq s < t} (X_u - X_{u-}) \quad (11)$$

where S_t^c represents the continuous part of (7) and X_{t-} means that the value of X_t just before a jump happens at time t . Now, we focus on the jump component for (11). According to the previous descriptions of the jumps, the percentage of the jump amplitude is e^j as long as the jump occurs at time u , that is, $S_u = e^j S_{u-}$. Thus, we obtain the following:

$$X_u - X_{u-} = \ln S_u - \ln S_{u-} = J \quad (12)$$

If the jump does not occur at time u , then $X_u - X_{u-} = 0$. In either case we have:

$$X_u - X_{u-} = J \Delta N_u \quad (13)$$

According to (13), the jump term is as follows:

$$\sum_{0 \leq s < t} (X_u - X_{u-}) = J \sum_{0 \leq s < t} \Delta N_u = \int_0^t J dN_u \quad (14)$$

Thus, the differential form of (11) is as follows:

$$\begin{aligned} dX_t &= \frac{1}{S_t} dS_t^c - \frac{1}{2} \frac{1}{S_t^2} dS_t^c dS_t^c + J dN_t \\ &= \kappa^* (\theta^* - X_t - \frac{\lambda m}{\kappa^*}) dt + \sqrt{v_t} dW_t^* - \frac{1}{2} v_t dt + J dN_t \end{aligned} \quad (15)$$

Based on equations (7)–(9) and (15), we obtain the following stochastic model for the log asset price:

$$dX_t = \kappa^* (\theta^* - X_t - \frac{v_t}{2\kappa^*} - \frac{\lambda m}{\kappa^*}) dt + \sqrt{v_t} dW_t^{1*} + J dN_t^* \quad (16)$$

$$dv_t = b^* (a^* - v_t) dt + \sigma v_t^{\eta/2} dW_t^{2*} \quad (17)$$

$$dW_t^{1*} dW_t^{2*} = \rho dt \quad (18)$$

V. OPTION PRICING: ANALITICAL AND NUMERICAL SOLUTIONS

In this section, we solve models (16)–(18) analytically to obtain the closed-form European option pricing formula with the characteristic function method proposed previously and its corresponding numerical solution based on the FFT algorithm.

A. Characteristic Function

First, the approximate characteristic function for the log underlying asset X_t is derived based on the following mathematical tools: stochastic analysis, differential equation, and perturbation analysis. The results calculated are illustrated in Theorem 1. The specific derivation details are shown in the appendix.

Theorem 1: We assume that the dynamic process of the log underlying asset $\{X_t, t \in [0, T]\}$ satisfies (16)–(18) under risk neutral measure $(\Omega, \mathcal{F}, \mathcal{Q})$ and $X_t = x$, $v_t = v$ at time $t \in [0, T]$. Then, the approximate conditional characteristic function for X_T is of the following form:

$$\phi_{X_T | \mathcal{F}_t}(y) \approx e^{B(t, T) + C(t, T)x + D(t, T)y + iyx} \quad (19)$$

where

$$C(t, T) = iy(e^{-\kappa^*(T-t)} - 1) \quad (20)$$

$$\begin{aligned} D(t, T) &= \frac{b^* - \kappa^* - \frac{\rho \sigma (1 + \eta) a^{\frac{\eta-1}{2}} iy}{2} e^{-\kappa^*(T-t)}}{\sigma^2 \eta a^{\eta(\eta-1)}} + \\ &\frac{2\kappa^* (\frac{se^{-\kappa^*(T-t)}}{2} - p) M(p, q, se^{-\kappa^*(T-t)})}{\sigma^2 \eta a^{\eta(\eta-1)} [M(p, q, se^{-\kappa^*(T-t)}) + C_0 W(p, q, se^{-\kappa^*(T-t)})]} + \\ &\frac{2\kappa^* (p + q + \frac{1}{2}) M(p + 1, q, se^{-\kappa^*(T-t)})}{\sigma^2 \eta a^{\eta(\eta-1)} [M(p, q, se^{-\kappa^*(T-t)}) + C_0 W(p, q, se^{-\kappa^*(T-t)})]} + \\ &\frac{2\kappa^* C_0 [(\frac{se^{-\kappa^*(T-t)}}{2} - p) W(p, q, se^{-\kappa^*(T-t)}) - W(p + 1, q, se^{-\kappa^*(T-t)})]}{\sigma^2 \eta a^{\eta(\eta-1)} [M(p, q, se^{-\kappa^*(T-t)}) + C_0 W(p, q, se^{-\kappa^*(T-t)})]} \end{aligned} \quad (21)$$

$$\begin{aligned} B(t, T) &= (\frac{\lambda m}{\kappa^*} - \theta^*) iy (e^{-\kappa^*(T-t)} - 1) + a^* b^* \int_t^T D(x, T) dx + \\ &\frac{1 - \eta}{2} a^* \eta \sigma^2 \int_t^T D^2(x, T) dx + \frac{\rho \sigma (1 - \eta) a^{\frac{\eta+1}{2}} iy}{2} \\ &\int_t^T e^{-\kappa^*(T-x)} D(x, T) dx + \int_t^T \Lambda(x, T) dx \end{aligned} \quad (22)$$

and

$$\begin{aligned} p &= \frac{a^{\frac{(\eta-1)}{2}} \sigma \eta i - (b^* - \kappa^*) \rho (1 + \eta) i}{2\kappa^* \sqrt{4\eta - \rho^2 (1 + \eta)^2}}, \quad q = -\frac{b^*}{2\kappa^*} \\ s &= -\frac{\sigma a^{\frac{(\eta-1)}{2}} y \sqrt{4\eta - \rho^2 (1 + \eta)^2}}{2\kappa^*}. \end{aligned}$$

where C_0 is a constant uniquely decided by the boundary value.

$M(\cdot, \cdot, \cdot)$ and $W(\cdot, \cdot, \cdot)$ are two Whittaker functions. These functions are two independent solutions to the well-known Whittaker equation and are available in Matlab software packages. These mathematical functions are widely applied in the fields of mathematics, physics, and engineering.

B. European Option Pricing Formula

Based on Theorem 1, we obtain the European option pricing formula using the method of characteristic function. The result is stated in Theorem 2. Though we use the European call option as an example, this method is also applicable to the European put option.

Theorem 2: We assume that the market of the underlying asset satisfies assumptions 1–3 and the underlying asset price follows the dynamics (7)–(9). Then, in the option market, the pricing formula for the European call option with delivery date T and exercise price K is as follows:

$$C(t, X_t, v_t; k, T) = e^{-r(T-t) - \alpha k} F_{k, u}^{-1} \left[\frac{\phi_{X_T | \mathcal{F}_t}(u - (\alpha + 1)i)}{\alpha^2 + \alpha - u^2 + i(2\alpha + 1)u} \right] \quad (23)$$

where $\phi_{X_T | \mathcal{F}_t}(y)$ is in the forms of (19)–(22) stated in Section V-A, α represents the modifying factor and $\alpha > 0$, $k = \ln K$. r is the short-term risk-free interest rate, and $F_{k, u}^{-1}(\cdot)$ represents the inverse Fourier transformation, as follows:

$$F_{k, u}^{-1}[g(u)] = \frac{1}{2\pi} \int_{-\infty}^{\infty} e^{-iuk} g(u) du$$

In particular, when $t = 0$, $C(0, X_0; k, T)$ is denoted by $C_T(k)$; $\psi(t, X_t; u, T)$ is denoted by $\psi_T(u)$; and $\phi_{X_T | \mathcal{F}_t}(y)$ is denoted by ϕ_T . We have the following:

$$C_T(k) = e^{-\alpha k} F_{k, u}^{-1} \left[\frac{e^{-rT} \phi_T(u - (\alpha + 1)i)}{\alpha^2 + \alpha - u^2 + i(2\alpha + 1)u} \right] \quad (24)$$

Proof: The conclusions are derived by directly applying the method of characteristic function proposed by Carr and Madan [3]. ■

TABLE III
THE PARAMETERS SETTING FOR SECTION VI-A

| Param | κ^* | θ^* | b^* | a^* | σ | ρ | p_u | q_d | n_1 |
|-------|------------|------------|----------|------------|-----------|--------|-------|-------|-------|
| Value | 10* | ln1.5 | 3.33 | 0.16 | 0.04 | 0.9 | 0.5 | 0.5 | 1 |
| n_2 | p_1 | q_1 | η_1 | θ_1 | λ | η | S_0 | v_0 | T |
| 1 | 1 | 1 | 2 | 2 | 0.11* | 1.1* | 1.3 | 0.18 | 1 |

The symbol “*” indicates that the corresponding values for the parameters are illustrated in the relevant figures when they are variables instead of constants, and we just omit them in the table for ease of presentation.

C. FFT-Based Numerical Solution

After obtaining the option pricing formula, we continue to derive the numerical solution based on the FFT algorithm. Without loss of generality, let $t=0$. It's well known that the FFT algorithm could reduce the operand from $O(N^2)$ to $O(N \log_2 N)$, which is a rather considerable reduction in the operation time. FFT is an efficient algorithm to calculate the sum in the following form:

$$w(h) = \sum_{j=1}^N e^{-\frac{2\pi}{N}(j-1)(h-1)} x(j), \quad h=1,2,\dots,N \quad (25)$$

Therefore, to adopt the FFT algorithm, transforming (24) into the summation form (25) is necessary. For ease of exposition, let

$$\varphi(u) = \frac{e^{-rT} \phi_T(u - (\alpha+1)i)}{\alpha^2 + \alpha - u^2 + i(2\alpha+1)u} \quad (26)$$

then (24) is simplified as follows:

$$C_T(k) = e^{-\alpha k} \Gamma_k^{-1}[\varphi(u)] = \frac{e^{-\alpha k}}{2\pi} \int_{-\infty}^{\infty} e^{-iuk} \varphi(u) du \quad (27)$$

The trapezoidal rule is applied to the right side of (27), and set:

$$u_j = \frac{1-N}{2} \Delta + (j-1)\Delta, \quad j=1,2,\dots,N.$$

Then, the approximate summation form of (27) is as follows:

$$C_T(k) \approx \frac{e^{-\alpha k}}{2\pi} \sum_{j=1}^N e^{-iu_j k} \varphi(u_j) \Delta \quad (28)$$

The upper bound of the integral at the right side of equation (28) is

$$q^* = \frac{N\Delta}{2}.$$

Let $k \in [-p^*, p^*]$ and set the step length as l , that is,

$$k_h = -p^* + l(h-1), \quad h=1,2,\dots,N \quad (29)$$

then $p^* = \frac{Nl}{2}$.

Substituted equation (29) into (28):

$$C_T(k_h) \approx \frac{e^{-\alpha k_h}}{2\pi} \sum_{j=1}^N e^{-i(\frac{1-N}{2}\Delta + (j-1)\Delta)(-p^* + l(h-1))} \varphi(u_j) \Delta \quad (30)$$

To transform (30) into the form in (25) so as to adopt the FFT algorithm, it must satisfy:

$$l\Delta = \frac{2\pi}{N} \quad (31)$$

Equation (31) is substituted into (30) to obtain:

$$C_T(k_h) \approx \frac{\Delta e^{-\alpha k_h}}{2\pi} e^{\frac{N-1}{2} \Delta k_h i} \sum_{j=1}^N e^{-\frac{2\pi}{N}(j-1)(h-1)} e^{ip^*(j-1)\Delta} \varphi(u_j) \quad (32)$$

where $h=1,2,\dots,N$, and

$$\varphi(u_j) = \frac{e^{-rT} \phi_T(u_j - (\alpha+1)i)}{\alpha^2 + \alpha - u_j^2 + i(2\alpha+1)u_j} \quad (33)$$

Thus far, (33) has been successfully transformed into the form in (25). Next, we could call the FFT algorithm from MATLAB to calculate the price of the European option very quickly.

TABLE IV
THE PARAMETERS SETTING FOR SECTION VI-B

| Param | b^* | κ^* | σ | ρ | η_1 | p_u | r | λ | p_1 |
|-------|-------|------------|------------|--------|----------|------------|-------|-----------|-------|
| Value | 3.33 | 10* | 0.04 | 0.9 | 2 | 0.5 | 0.05 | 0.11* | 1 |
| n_1 | n_2 | a^* | θ^* | v_0 | S_0 | θ_1 | q_d | η | T |
| 1 | 1 | 0.16 | 0.40339 | 0.18 | 1.3 | 2 | 0.5 | 1.1* | 1 |

The symbol “*” indicates that the corresponding values for the parameters are illustrated in the relevant figures when they are variables instead of constants, and we just omit them in the table for ease of presentation.

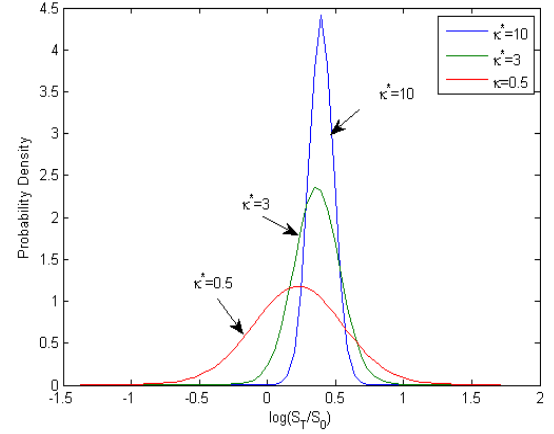


Fig. 4. Probability density function for different values of κ^* .

VI. NUMERICAL EXPERIMENT

In this section, we conduct several numerical experiments to verify both the modeling and solution methodology proposed in this paper. To validate the proposed model, we need to show whether the model could characterize the simultaneous properties of mean reversion, jumps, volatility smile, and leptokurtosis and fat tail observed in some markets. It is obvious that the basic model theoretically contains characteristics of mean reversion and jumps, thus we only have to conduct analysis on the probability density function and volatility of the underlying asset to see whether the model could reflect the market properties of leptokurtosis and fat tail and volatility smile. We also need to test the validity of the solution methodology. To do that, we compare the effects of the FFT-based numerical solution proposed in this paper with the traditional Differential Monte Carlo (DMC) simulations. All the experiments are implemented on a Pentium Dual 2.0 GHz/2.0 GB personal computer under a Windows XP Professional 2002 version operating system running MATLAB R2012a. For each experiment, the parameters are selected with reference to a previous study [20], and the specific settings are illustrated in each part.

A. Probability Density Functions Analysis

The probability density function of the log underlying asset return can be obtained by inverting Fourier transform on the characteristic function (19). Based on the capacity of addressing a large amount of data quickly, the FFT algorithm makes it possible to conduct numerical simulations on the probability density function of the log return and examine the properties reflected by the proposed model. All the parameters values are presented in Table III and the impacts of κ^* , λ , b^* , and η on the distribution shape are illustrated in Figs. 4 through 7. We see that all the distributions show the property of leptokurtosis and fat tail, which is consistent with the characteristics

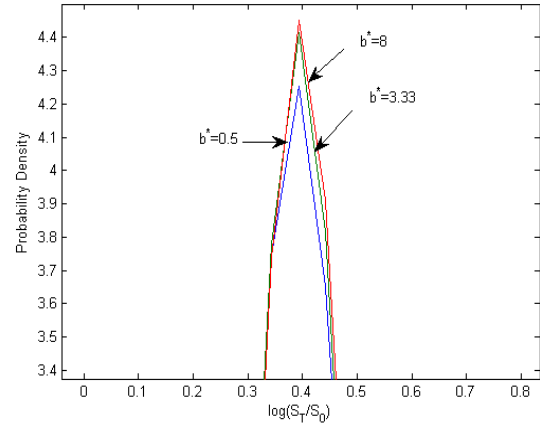
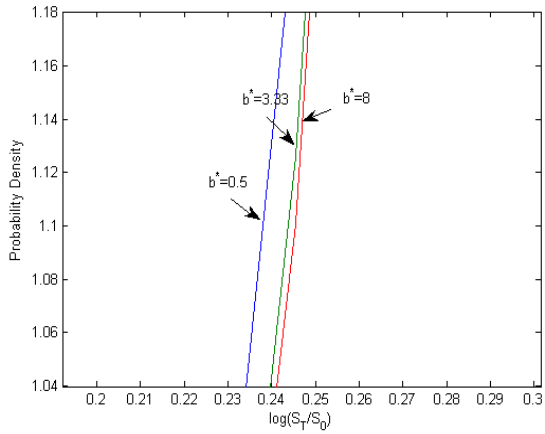
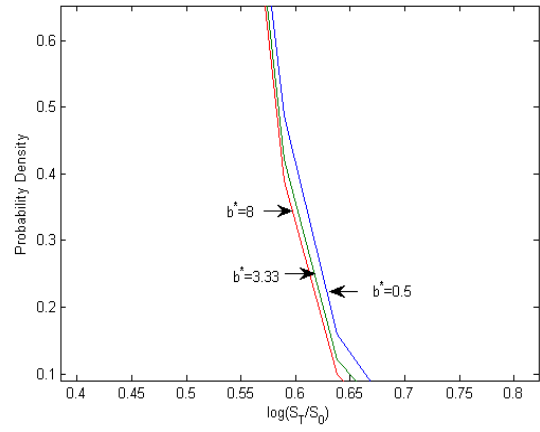
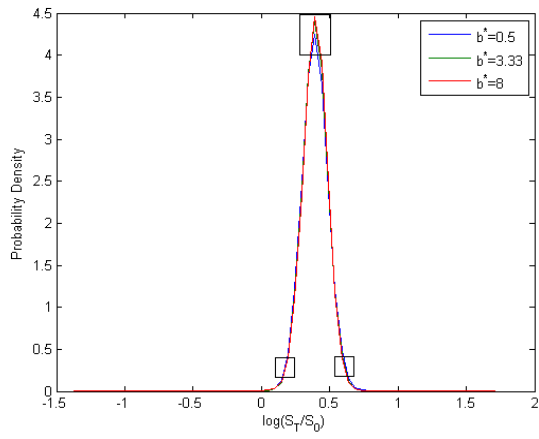


Fig.5. Probability density functions of the log return of the underlying asset for different values of b^* .

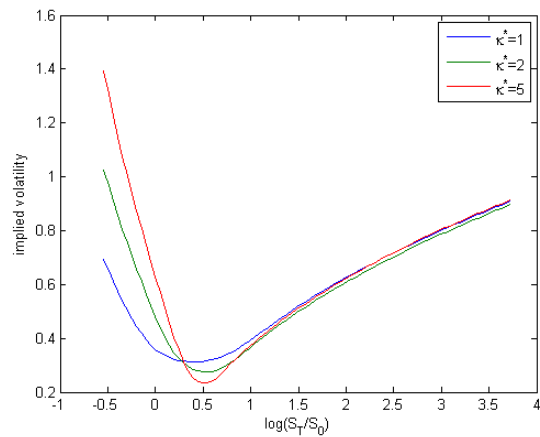
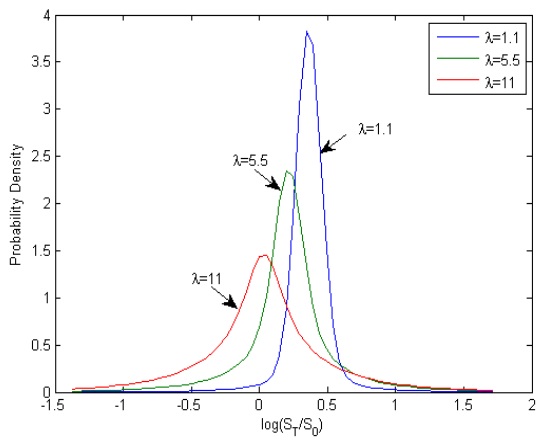


Fig. 6. Probability density functions for different values of λ .

Fig.8. Implied volatility smile/skew for different values of κ^* .

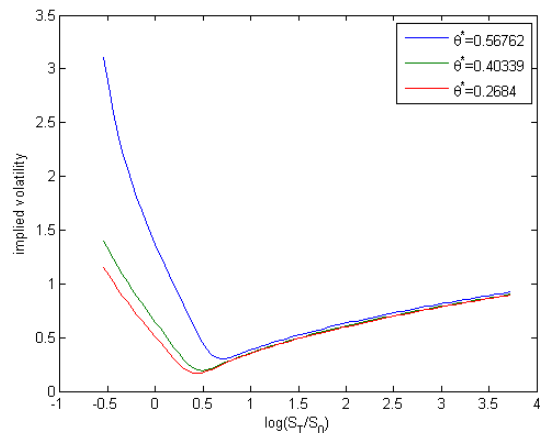
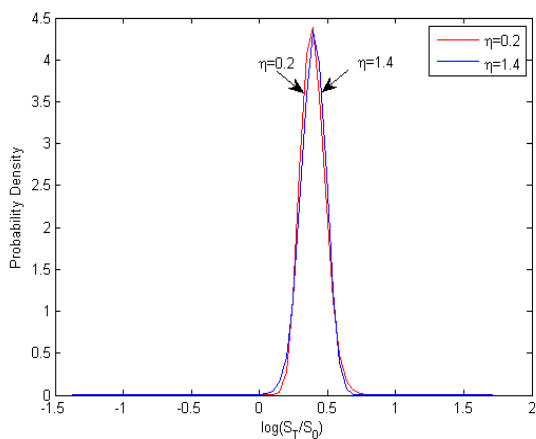


Fig. 7. Probability density functions for different values of η .

Fig. 9. Implied volatility smile/skew for different values of θ^* .

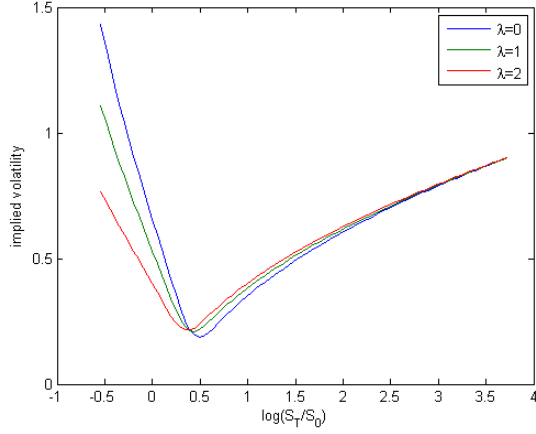


Fig. 10. Implied volatility smile for different values of λ .

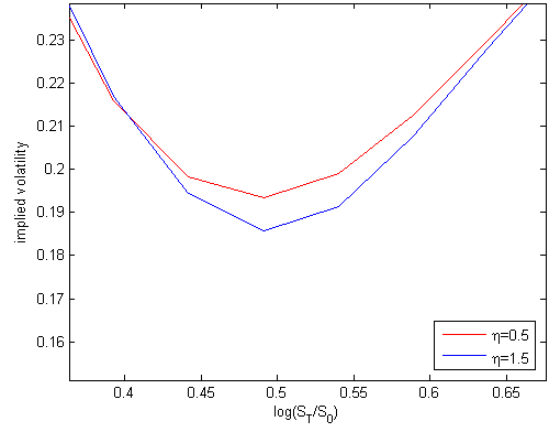


Fig. 11. Probability density functions for different values of η .

of big data fitting in our empirical study and further validates the effectiveness of our model.

Fig. 4 shows how the mean reversion rate of the underlying asset pushes the distribution more towards the equilibrium mean level θ^* . When the log return deviates from its equilibrium level θ^* , a larger reverting rate helps the log return back to the equilibrium level faster. Consequently, the variance of the distribution is smaller. As shown in Fig. 4, the shape of the distribution is more concentrated when the mean reversion rate of the log return is larger, which verifies the theoretical analysis. In real financial markets, a larger κ^* means a stronger external intervention. For example, in the Chinese market, κ^* may prove to be larger than that obtained in overseas markets because the Chinese government intervenes more in the economy to maintain its stability.

Fig. 5 shows how the mean reverting rate of the volatility process affects the shape of the distribution. A larger value of b^* means a faster reverting speed for the volatility to its equilibrium level a^* . In our example, the initial volatility value is larger than the equilibrium level. Thus, a quick reverting rate creates a smaller variance of the log return. Moreover, we can observe that a larger b^* makes the distribution more concentrated and have a thinner tail. If the initial value of the volatility is smaller than the equilibrium level, the case will be the opposite and the distribution will have a fatter tail.

The way by which jump intensity λ affects the distribution of the log return is shown in Fig. 6. A larger value of λ means that more jumps can occur at a certain time, causing larger volatility of the underlying asset's log return, resulting in a bigger variance of the log return. As seen in Fig. 6, the distribution of the log return is more concentrated with smaller jump intensity λ , which is consistent with the theoretical analysis. For instance, during a financial crisis, the jump intensity can be larger as the disturbance of the financial market increases.

The relationship between the non-affine volatility coefficient of the volatility process η and the log return of the underlying asset is shown in Fig. 7. From Fig. 7, we can see that little differences exist between the probability density functions with different non-affine coefficients under our parameters setting. However, a larger value of η creates a fatter left tail and a thinner right tail of the log return's distribution. A bigger volatility's volatility item results in a smaller volatility (variance) of the log return. When the variance of the log asset is large enough, the volatility's volatility item increases in η , and when the variance is small enough, it decreases in η . Therefore,

when the spot asset's price is relatively small, a larger η will make a larger variance of the log return, thereby fattening the left tail of the density function and vice versa.

B. Implied Volatility Smile Analysis

Based on the accurate FFT algorithm, we could further investigate the famous "volatility smile" phenomenon implied by the proposed model. All parameters settings are presented in Table IV and the impacts of κ^* , θ^* , λ , and η on the implied volatility are illustrated in Figs. 8 through 11.

The way by which the implied volatility curve reacts to the different values of κ^* is shown in Fig. 8. The left-tail skew of the volatility smile increases with κ^* , and as κ^* approaches zero, the volatility smile tends to be symmetrical.

The relationship between the long-term equilibrium level of the log return of the underlying asset θ^* and the volatility smile is shown in Fig. 9. From Fig. 9, we can observe that the left-tail skew increases with the equilibrium value θ^* . A positive correlation coefficient ρ leads to a high variance when the price of the underlying asset rises. Moreover, the price of the underlying asset increases with the equilibrium value θ^* . Therefore, a larger θ^* results in larger variance of the log return, thereby leading to larger implied volatility.

Fig. 10 shows how the jump intensity λ influences the implied volatility smile. We see that when the price of log return is larger than a certain value, the implied volatility increases as the jump intensity decreases. When the price of the log return is smaller than a certain value, the implied volatility decreases, whereas the jump intensity increases.

Fig. 11 shows the effect of the non-affine volatility coefficient of the volatility process η to the implied volatility smile. When the price of the log return of the underlying asset is smaller than some point, a larger non-affine coefficient η leads to a larger implied volatility. The opposite case is observed when the price of the log return is bigger than that point.

C. Comparison between FFT and DMC

To verify the efficiency and effectiveness of our proposed method, we use two numerical algorithms to calculate the European call option prices. One is the DMC simulation method based on the dynamic model of the underlying asset price (16)–(18) and the other is the FFT algorithm based on the numerical solutions proposed in Section V. Using the results calculated by DMC as a benchmark, we compare

TABLE V
PARAMETERS VALUES FOR SECTION VI-C

| | | | | | | | | |
|-------|------------|------------|----------|------------|----------|----------|----------|-------|
| Param | κ^* | θ^* | a^* | b^* | σ | ρ | η | r |
| Value | 10 | 0.40339 | 0.16 | 3.33 | 0.04 | 0.9 | 0.5 | 0.05 |
| Param | S_0 | v_0 | T | λ | p_u | p_d | n_1 | n_2 |
| Value | 1.3 | 0.18 | 1 | 0.11 | 0.5 | 0.5 | 1 | 1 |
| Param | p_1 | q_1 | η_1 | θ_1 | N | α | Δ | M |
| Value | 1 | 1 | 2 | 2 | 512 | 1.5 | 0.25 | 50000 |

FFT with DMC on both accuracy and operation time. All the parameters used are shown in Table V.

DMC computes the option price based on the following principle:

$$C_0 = E^Q[e^{-rT} C_T | S_0, v_0] = E^Q[e^{-rT} (S_T - K)^+ | S_0, v_0] \quad (34)$$

where C_0 denotes the European call option price at $t=0$, S_0 and v_0 respectively represent the underlying asset price and volatility at $t=0$, and the other symbols are similar to that in the previous sections.

The specific steps for DMC simulation are as follows. First, S_T is obtained with the difference method based on S_0 , v_0 , and models (16)–(18). Then, the European option price C_0 is calculated by the Monte Carlo simulation based on (34), with the idea of using mean values to approximate the expectation, that is,

$$C_0 = e^{-rT} \frac{1}{M} \sum_{i=1}^M \max\{S_T^{(i)} - K, 0\} \quad (35)$$

Using DMC simulation and FFT algorithm to calculate the European option prices with different exercise prices, we obtain the final European option prices in comparison in Table VI. (We select 10 values from the 512 option prices as represented here.)

Table VI shows a comparison of the European option prices calculated by FFT and DMC. A total of 512 evenly-spaced points in the interval $k \in [-4\pi, 4\pi]$, representing 512 different log exercise prices for options with the same underlying asset and delivery time, are selected. As seen in Table VI, the European option prices increase with the exercise prices obtained by either FFT or DMC, which is consistent with the option pricing theory. On the other hand, with the option prices computed by DMC as benchmark, the maximum error of results calculated by the FFT is around 0.0708, thereby demonstrating that the FFT numerical solution based on the triple characteristic model is accurate. More importantly, running the FFT algorithm to compute all of the 512 option prices only takes a total of about 12.97 min, whereas computing one single option price by DMC when adopting 50000 paths to approximate the true value takes about 2.47 min. After this comparison, we conclude that when multiple risks exist in the market, the traditional Monte Carlo simulation is no longer a viable method in practice, especially when the data is big. On the contrary, the FFT numerical solution is an efficient tool to address multiple risks and big data.

VII. CONCLUSION

In the big data era, option pricing becomes more challenging because data are collected in higher frequency and in larger amounts. This requires more general pricing models that fit the characteristics of big data better and adaptable algorithms to calculate the option prices faster. Through empirical evidences, we show that the phenomena of mean reversion, jumps, volatility smile, and leptokurtosis and fat tail simultaneously occur in certain kinds of

markets such as the

TABLE VI
EUROPEAN CALL PRICES WITH DIFFERENT EXERCISE PRICES:
FFT VS DMC

| Exercise price | FFT | DMC | Errors |
|----------------|-------------|-------------|-------------|
| 0.821725 | 0.949253076 | 0.886697463 | 0.070548993 |
| 0.863068 | 0.918218627 | 0.857520099 | 0.070783795 |
| 0.90649 | 0.886174482 | 0.842281112 | 0.052112494 |
| 0.952098 | 0.8530305 | 0.80792565 | 0.055827972 |
| 1.000000 | 0.818694917 | 0.775975186 | 0.055052961 |
| 1.050312 | 0.783074085 | 0.740406464 | 0.057627295 |
| 1.103156 | 0.746072215 | 0.702606974 | 0.061862808 |
| 1.158658 | 0.707591128 | 0.669813408 | 0.056400364 |
| 1.216952 | 0.667530033 | 0.632033519 | 0.056162392 |
| 1.342488 | 0.62578531 | 0.594622191 | 0.052408267 |

currency option market. To provide a good pricing tool for this kind of market, this paper considers the European option pricing problem in a general case when the underlying asset follows a stochastic process containing properties of mean reversion, non-affine stochastic volatility, and mixed-exponential jumps. With the characteristic function method, the European option pricing formula is obtained and the numerical solution based on the FFT algorithm is obtained. Through extensive numerical experimentation, the model proposed in this paper is shown to be effective in capturing the multiple features in the market, and the FFT algorithm is also shown to be both accurate and efficient even with big data.

Our work has several limitations. First, to simplify our model, we have used three limiting assumptions on the risk-free interest rate, transaction cost and market dividends. Based on the modeling structure and solution methodology, we could, in further research, consider European option pricing problems using empirical methods by extending these assumptions for better pricing accuracy quantitatively besides characterizing the properties of the market qualitatively. Secondly, in addition to the multiple kinds of objective risks considered in this paper, subjective fuzziness also exists in the market [21]. Therefore, further research can be done to study the option pricing problems in the presence of both randomness and fuzziness. Except for vanilla European option, many other kinds of exotic options, such as barrier, Asian, and look-back options, are also worth exploring in the future.

APPENDIX

Proof of Theorem 1 The characteristic function of X_T satisfying (16)–(18) is defined as:

$$f(t, x, v; y) = E^Q[e^{iyX_T} | X_t = x, v_t = v] \quad (A1)$$

According to the generalized Feynman-Kac theorem, $f(y; t, x, v)$ is a solution to the integral partial differential equation (IPDE), as follows:

$$\begin{aligned} \frac{\partial f}{\partial t} + \kappa^*(\theta^* - x - \frac{v}{2\kappa^*} - \frac{\lambda m}{\kappa^*}) \frac{\partial f}{\partial x} + \frac{1}{2} v \frac{\partial^2 f}{\partial x^2} + b^*(a^* - v) \frac{\partial f}{\partial v} + \frac{1}{2} \sigma^2 v^\eta \frac{\partial^2 f}{\partial v^2} \\ + \rho \sigma v^{\frac{\eta+1}{2}} \frac{\partial^2 f}{\partial x \partial v} + \lambda \int_{-\infty}^{+\infty} [f(t, x+z, v; y) - f(t, x, v; y)] g_J(z) dz = 0 \end{aligned} \quad (A2)$$

with boundary condition:

$$f(T, x, v; y) = e^{iyx} \quad (A3)$$

where $g(J)$ is the distribution function of the stochastic variable J .

According to the coefficients of each term in (A2), we know that (A2) is a non-affine IPDE and the analytical solution cannot be obtained as a rule. Here, we utilize a perturbation method [22] to derive an approximate solution. The main feature of the method relies

on approximating v^η and $v^{\frac{\eta+1}{2}}$ in the PIDE using Taylor expansion around a^* , which is the long-term mean value of the volatility process, as follows:

$$v^\eta = (v - a^* + a^*)^\eta \approx C_\eta^0 a^{*\eta} + C_\eta^1 a^{*(\eta-1)}(v - a^*) \\ = (1 - \eta)a^{*\eta} + \eta a^{*(\eta-1)}v \quad (\text{A4})$$

$$v^{\frac{\eta+1}{2}} = (v - a^* + a^*)^{\frac{\eta+1}{2}} \approx a^{*\frac{\eta+1}{2}} + \frac{\eta+1}{2} a^{*\frac{\eta-1}{2}}(v - a^*) \\ = \frac{1-\eta}{2} a^{*\frac{\eta+1}{2}} + \frac{\eta+1}{2} a^{*\frac{\eta-1}{2}}v \quad (\text{A5})$$

These approximations result in the following PIDE:

$$\frac{\partial f}{\partial t} + \kappa^*(\theta^* - x - \frac{v}{2\kappa^*} - \frac{\lambda m}{\kappa^*}) \frac{\partial f}{\partial x} + \frac{1}{2}v \frac{\partial^2 f}{\partial x^2} + b^*(a^* - v) \frac{\partial f}{\partial v} + \\ \frac{1}{2}\sigma^2((1-\eta)a^{*\eta} + \eta a^{*(\eta-1)}v) \frac{\partial^2 f}{\partial v^2} + \rho\sigma(\frac{1-\eta}{2} a^{*\frac{\eta+1}{2}} + \frac{\eta+1}{2} a^{*\frac{\eta-1}{2}}v) \quad (\text{A6}) \\ \frac{\partial^2 f}{\partial x \partial v} + \lambda \int_{-\infty}^{+\infty} [f(t, x+z, v; y) - f(t, x, v; y)] g_J(z) dz = 0$$

As the coefficients of the stochastic differential equations (SDE) (16)–(17) are all linear, according to the theories of linear partial differential equation, the solution to IPDE (A6) $f(t, x, v; y)$ has the following exponential form:

$$f(t, x, v; y) = e^{B(t,T) + C(t,T)x + D(t,T)v + iyx} \quad (\text{A7})$$

where $B(t, T)$, $C(t, T)$, and $D(t, T)$ are the deterministic functions of t . Through boundary condition (A3), we have:

$$B(T, T) = 0, \quad C(T, T) = 0, \quad D(T, T) = 0 \quad (\text{A8})$$

Next, we consider the integral term in (A6):

$$\lambda \int_{-\infty}^{+\infty} [f(t, x+z, v; y) - f(t, x, v; y)] g_J(z) dz = f(t, x, v; y) \Lambda(t, T) \quad (\text{A9})$$

where

$$\Lambda(t, T) = \lambda \int_{-\infty}^{+\infty} (e^{(C(t,T)+iy)z} - 1) g_J(z) dz \\ = \lambda (p_u \sum_{i=1}^{n_1} \frac{p_i \eta_i}{\eta_i - iy - C(t, T)} + q_d \sum_{j=1}^{n_2} \frac{q_j \theta_j}{\theta_j + iy + C(t, T)} - 1)$$

The derivation process is based on the fact that the stochastic variable J representing the percentage of jump amplitude is independent from the stochastic process X_t and $J \sim MEJ(p_u, p_i, \eta_i, q_d, q_j, \theta_j)$.

By simplification, we obtain the following equation:

$$[B_t(t, T) + (\kappa^* \theta^* - \lambda m)(C(t, T) + iy) + a^* b^* D(t, T) + \frac{1-\eta}{2} a^{*\eta} \sigma^2 D^2(t, T) \\ + \frac{\rho\sigma(1-\eta)}{2} a^{*\frac{\eta+1}{2}} (C(t, T) + iy) D(t, T) + \Lambda(t, T)] + [C_t(t, T) - \kappa^* (C(t, T) \\ + iy)]x + [D_t(t, T) + \frac{1}{2}(C(t, T) + iy)(C(t, T) + iy - 1) - b^* D(t, T) + \\ \frac{1}{2}\sigma^2 \eta a^{*(\eta-1)} D^2(t, T) + \frac{\rho\sigma(1+\eta)}{2} a^{*\frac{\eta-1}{2}} (C(t, T) + iy) D(t, T)]v = 0 \quad (\text{A10})$$

As equation (A10) holds true for any t and x , in definition domains, we have:

$$B_t(t, T) + (\kappa^* \theta^* - \lambda m)(C(t, T) + iy) + a^* b^* D(t, T) + \frac{1-\eta}{2} a^{*\eta} \sigma^2 \quad (\text{A11})$$

$$D^2(t, T) + \frac{\rho\sigma(1-\eta)}{2} a^{*\frac{\eta+1}{2}} (C(t, T) + iy) D(t, T) + \Lambda(t, T) = 0$$

$$C_t(t, T) - \kappa^* (C(t, T) + iy) = 0 \quad (\text{A12})$$

$$D_t(t, T) + \frac{1}{2}(C(t, T) + iy)(C(t, T) + iy - 1) - b^* D(t, T) + \frac{1}{2}\sigma^2 \eta \\ a^{*(\eta-1)} D^2(t, T) + \frac{\rho\sigma(1+\eta)}{2} a^{*\frac{\eta-1}{2}} (C(t, T) + iy) D(t, T) = 0 \quad (\text{A13})$$

where $B(t, T)$, $C(t, T)$ and $D(t, T)$ satisfy the boundary conditions in (A8).

According to Zwillinger (1992), $B(t, T)$, $C(t, T)$ and $D(t, T)$ are easily solved from equations (A11)–(A13), and the specific forms are just illustrated in Section V-A. ■

REFERENCES

- [1] F. Black, and M. Scholes, "The pricing of options and corporate liabilities," *Journal of political economy*, vol. 81, pp. 637-654, 1973.
- [2] S. L. Heston, "A closed-form solution for options with stochastic volatility with applications to bond and currency options," *The Review of Financial Studies*, vol. 6, no. 2, pp. 327-343, 1993.
- [3] P. Carr, and D. B. Madan, "Option valuation using the fast Fourier transform," *Journal of computational finance*, vol. 2, no. 4, pp. 61-73, 1999.
- [4] Tsan-Ming Choi, "Coordination and risk analysis of VMI supply chains with RFID technology," *IEEE Trans. Industrial Informatics*, vol. 7, no. 3, pp. 497-504, Jul. 2011.
- [5] S. C. Muller, U. Hager, and C. Rehtanz, "A multiagent system for adaptive power flow control in electrical transmission systems," *IEEE Trans. Industrial Informatics*, vol. 10, no. 4, pp. 2290-2299, Apr. 2014.
- [6] S. Asian, and X. Nie, "Coordination in supply chain with uncertain demand and disruption risks: existence, analysis, and insights," *IEEE Trans. Systems, Man, and Cybernetics: Systems*, vol. 44, no. 9, pp. 1139-1154, Sep. 2014.
- [7] Wenbo Shi, and K. J. Min, "Product remanufacturing: a real options approach," *IEEE Trans. Engineering Management*, vol. 61, no. 2, pp. 237-250, May 2014.
- [8] W. J. Hahn, and J. S. Dyer, "Discrete time modeling of mean-reverting stochastic processes for real option valuation," *European Journal of Operational Research*, vol. 184, no. 2, pp. 534-548, 2008.
- [9] S. H. Park, and J. H. Kim, "A semi-analytic pricing formula for look back options under a general stochastic volatility model," *Statistics & Probability Letters*, vol. 83, no. 11, pp. 2537-2543, 2013.
- [10] C. H. Yuen, and W. Zheng, "Pricing exotic discrete variance swaps under the 3/2- stochastic volatility models," *Applied Mathematical Finance*, pp. 1-29, 2015.
- [11] F. A. Fard, "Analytical pricing of vulnerable options under a generalized jump-diffusion model," *Insurance: Mathematics and Economics*, vol. 60, pp. 19-28, 2015.
- [12] S. F. Chung, and H. Y. Wong, "Analytical pricing of discrete arithmetic Asian options with mean reversion and jumps," *Journal of Banking & Finance*, vol. 44, pp. 130-140, 2014.
- [13] K. Mayer, and T. Schmid, F. Weber, "Modeling electricity spot prices: combining mean reversion, spikes, and stochastic volatility," *The European Journal of Finance*, vol. 21, no. 4, pp. 292-315, 2015.
- [14] N. Gradojevic, R. Gençay, and D. Kukulj, "Option pricing with modular neural networks," *IEEE Trans. Neural Networks*, vol. 20, no. 4, pp. 626-637, Apr. 2009.
- [15] Anson H. T. Tse, D. Thomas, and W. Luk, "Design exploration of quadrature methods in option pricing," *IEEE Trans. Very Large Scale Integration Systems*, vol. 20, no. 5, pp. 818-826, May 2012.
- [16] E. Zhou, "Optimal stopping under partial observation: near-value iteration," *IEEE Trans. Automatic Control*, vol. 58, no. 2, pp. 500-506, Feb. 2013.
- [17] J. Selva, "FFT interpolation from nonuniform samples lying in a regular grid," *IEEE Trans. Signal Processing*, vol. 63, no. 11, pp. 2826-2834, Jun. 2015.
- [18] H. Wen, J. Zhang, Z. Meng, et al., "Harmonic estimation using symmetrical interpolation FFT based on triangular self-convolution window," *IEEE Trans. Industrial Informatics*, vol. 11, no. 1, pp. 16-26, Feb. 2015.
- [19] S. McKeown, and R. Woods, "Power efficient, FPGA implementations of transform algorithms for radar-based digital receiver applications," *IEEE Trans. Industrial Informatics*, vol. 9, no. 3, pp. 1501-1600, Aug. 2013.
- [20] H. Y. Wong, and Y. W. Lo, "Option pricing with mean reversion and stochastic volatility," *European Journal of Operational Research*, vol. 197, no. 1, pp. 179-187, 2009.
- [21] V. Behood, Jie Lu, and G. Zhang, "Fuzzy refinement domain adaptation for long term prediction in banking ecosystem," *IEEE Trans. Industrial Informatics*, vol. 10, no. 2, pp. 1637-1646, May 2014.
- [22] B. Heidergott, H. Leahu, and W. Volk-Makarewicz, "A Smoothed Perturbation Analysis of Parisian Options," *IEEE Trans. Automatic Control*, vol. 60, no. 2, pp. 469-474, Feb. 2015.

